ResearchGate

See discussions, stats, and author profiles for this publication at: https://www.researchgate.net/publication/237058840

# Surface-Induced Diastereomeric Complex Formation of a Nucleoside at the Liquid/Solid Interface: Stereoselective Recognition and Preferential Adsorption

**ARTICLE** *in* JOURNAL OF THE AMERICAN CHEMICAL SOCIETY · JUNE 2013

Impact Factor: 12.11 · DOI: 10.1021/ja402914m · Source: PubMed

CITATIONS
11

READS
39

**14 AUTHORS**, INCLUDING:

Zongxia Guo
Qingdao University of Science and Technology

**20** PUBLICATIONS **192** CITATIONS

SEE PROFILE

Bernard Van Averbeke
Université de Mons

**19** PUBLICATIONS **545** CITATIONS

SEE PROFILE

Roberto Lazzaroni
Université de Mons

**400** PUBLICATIONS **9,343** CITATIONS

SEE PROFILE

Albertus P H J Schenning
Technische Universiteit Eindhoven

**295** PUBLICATIONS **14,360** CITATIONS

SEE PROFILE

Available from: Albertus P H J Schenning
Retrieved on: 24 January 2016

JACS
JOURNAL OF THE AMERICAN CHEMICAL SOCIETY
Article
pubs.acs.org/JACS

# Surface-Induced Diastereomeric Complex Formation of a Nucleoside at the Liquid/Solid Interface: Stereoselective Recognition and Preferential Adsorption

Zongxia Guo,[†,∥] Inge De Cat,[†] Bernard Van Averbeke,[§] Elke Ghijsens,[†] Jianbin Lin,[‡] Hong Xu,[†] Guojie Wang,[†,#] Freek J. M. Hoeben,[‡] Željko Tomović,[‡] Roberto Lazzaroni,*[,§] David Beljonne,[§] E. W. Meijer,[‡] Albertus P. H. J. Schenning,*[,‡,⊥] and Steven De Feyter*[,†]

[†]Division of Molecular Imaging and Photonics, Department of Chemistry, KU Leuven, Celestijnenlaan 200 FB-3001, Leuven, Belgium

[‡]Laboratory of Macromolecular and Organic Chemistry, Eindhoven University of Technology, P.O. Box 513, 5600 MB Eindhoven, The Netherlands

[§]Service de Chimie des Materiaux Nouveaux, Université de Mons-UMONS, Place du Parc 20, 7000 Mons, Belgium

[∥]Qingdao Institute of Bioenergy and Bioprocess Technology, Chinese Academy of Sciences, 189 Songling Road, 266101, Qingdao, People's Republic of China

Supporting Information

**ABSTRACT:** With the aim of achieving surface-mediated enantioselective adsorption, the self-assembly of chiral oligo(*p*-phenylenevinylene) (OPV3T) with nucleosides is investigated at the liquid/solid interface by means of scanning tunneling microscopy and molecular modeling. OPV3T enantiomers form mirror related hexameric rosette patterns. The DNA nucleoside, thymidine, does not self-assemble into stable adlayers but coadsorbs with OPV3T on the surface, leading to a pattern transformation of OPV3T from rosettes to dimers, and a change in chiral expression as well. Diastereoselective recognition between OPV3T and thymidine enantiomers can be used to resolve thymidine enantiomers at an achiral surface with an OPV3T enantiomer as the resolving agent. The impact of molar ratio and concentration on the self-assembly and chiral resolution is systematically investigated. Because there is no interaction between OPV3T and thymidine in solution, the liquid/solid interface acts as the platform for the chiral resolution of thymidine enantiomers.

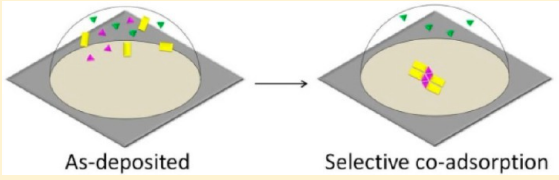


## INTRODUCTION

The separation of a racemate into its enantiomers (resolution) is of great importance in pharmaceutical and materials technologies.[1−4] The interaction of molecules with interfaces provides interesting opportunities to resolve chiral molecules.[5−18] While in solution only 5−10% of all racemates crystallize as a conglomerate (i.e., the enantiomers crystallize as separate phases),[19] on surfaces it seems that the majority of the racemates self-assembling into monolayers organize into enantiomorphous domains.[20−27] Despite pronounced conglomerate formation on surfaces, isolation and collection of the enantiomers remains a very difficult task, as the domain size is often at the nanometer scale.[28] From a practical point of view, selective adsorption or crystallization of one of the enantiomers on surfaces is more relevant for separation purposes.[29−31]

In this study, we explore in detail structural and dynamic aspects, and concentration- and ratio-dependent effects of surface-mediated diastereoselective recognition and adsorption. In particular, we investigate the unprecedented situation in which a chiral resolving agent and chiral compound do not interact in solution, but only form a complex upon confinement on a surface. Furthermore, the resolving agent is interacting stronger with one of the enantiomers upon surface-confinement; one of the so-formed diastereomers is more stable. Following this difference in stability, a diastereomeric complex formed by one of the enantiomers of the racemate and resolving agent is preferentially formed and adsorbed on a surface as a self-assembled monolayer. The other enantiomer is left in solution.

A versatile tool to explore molecular self-assembly and chirality aspects on atomically flat conductive surfaces is scanning tunneling microscopy (STM). Even at liquid/solid interfaces, STM has the potential to shine light on the structural and dynamic aspects of chiral recognition,[32−45] induction,[46−55] and separation processes on surfaces,[16] with submolecular resolution.

We selected chiral oligo-(*p*-phenylenevinylene) derivatives with a diaminotriazine headgroup (OPV3T) and thymidine enantiomers (Figure 1) to explore surface-mediated diastereoselective recognition and adsorption at the interface between a solvent (1-octanol) and an atomically flat substrate (highly

**Received:** March 22, 2013
**Published:** June 6, 2013

 © 2013 American Chemical Society 

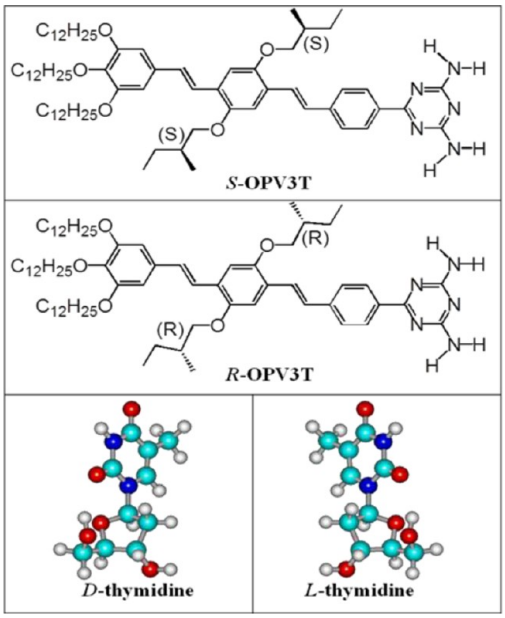


**Figure 1.** Structures of *S*-OPV3T, *R*-OPV3T, D-thymidine, and L-thymidine.

oriented pyrolytic graphite (HOPG)). The $\pi$-conjugated OPV moieties act as markers, facilitating the identification of the supramolecular architectures by STM. Thymidine is a DNA nucleoside. OPV3T and thymidine have complementary hydrogen-bonding sites, which can promote strong intermolecular interactions and coadsorption at the interface.[55] Thymidine coadsorbs with OPV at the interface and induces morphological changes of the supramolecular architectures, which depend on the concentration and molar ratio. The thymidine enantiomers can be resolved at the liquid/solid interface using OPV3T enantiomers as the resolving agent because of chiral selective recognition and preferential adsorption of one of the supramolecular diastereomers on the solid surface, leading under optimized conditions to an enantiomeric excess (ee) of 90%.

## ■ RESULTS AND DISCUSSION

**Self-Assembly of Chiral OPV3T at 1-Octanol/HOPG Interface.** In the first stage, we explored the self-assembly of the OPV3T pure enantiomers at the 1-octanol/HOPG interface. Similar to previous reports on the self-assembly of *S*-OPV3T at the 1-phenyloctane/HOPG interface,[56,57] both enantiomers form monolayers, which are composed of several crystalline domains, the result of many nucleation sites (Supporting Information S1). Figure 2a and b shows high-resolution STM images of part of an *S*-OPV3T and *R*-OPV3T domain at the 1-octanol/HOPG interface, respectively. The bright rods correspond to the conjugated OPV backbone, while the dodecyloxy chains appear as less bright lines. Only two out of three alkyl chains per OPV3T molecule are adsorbed on the HOPG surface, for sterical reasons. The third one is directed to and probably solvated by the supernatant solution. Both enantiomers assemble into ordered monolayers of cyclic hexameric structures, called "rosettes". The 1,3-diaminotriazine groups point to the core of the rosette and stabilize the supramolecular unit via hydrogen bonds. Adjacent rosettes interact via van der Waals interactions between alkyl chains. The unit cell parameters for both enantiomers are the same

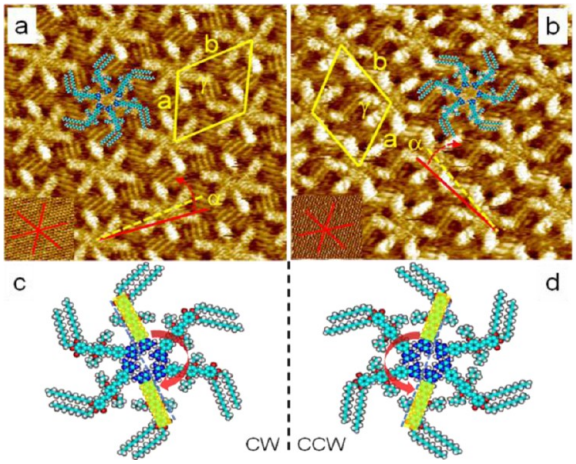


**Figure 2.** STM-images of chiral OPV3T at the 1-octanol/HOPG interface. (a) *S*-OPV3T, $I_{set}$ = 0.448 nA, $V_{set}$ = −0.43 V. (b) *R*-OPV3T, $I_{set}$ = 0.68 nA, $V_{set}$ = −0.28 V. In (a) and (b), red solid lines reflect symmetry axes of graphite, and yellow dotted lines run parallel to unit cell vector *b*. Insets are images of HOPG, recorded underneath the monolayer. In each of the images, a rosette model is superimposed. (c,d) Rosette models. (c) Clockwise (CW) rosette from *S*-OPV3T. (d) Counterclockwise (CCW) rosette from *R*-OPV3T. [OPV3T] = 1.0 mM. Size of STM images is 20 × 20 nm$^2$.

within experimental error: $a$ = 5.49 ± 0.12 nm, $b$ = 5.47 ± 0.11 nm, $\gamma$ = 119 ± 2° for *S*-OPV3T and $a$ = 5.45 ± 0.10 nm, $b$ = 5.50 ± 0.09 nm, $\gamma$ = 120 ± 2° for *R*-OPV3T. The packing patterns are not identical though. The rosettes are chiral, not only because they are composed of chiral molecules, but also because of the arrangement of the OPV3T molecules within one rosette.[58] Close inspection reveals a lateral offset for the opposite OPV units within one rosette that are collinear, the direction of which is enantiomer dependent. The chirality of these rosettes is also nicely demonstrated by the orientation of the alkyl chains. We label *S*-OPV3T rosettes as clockwise (CW) and *R*-OPV3T rosettes as counterclockwise (CCW). Furthermore, both enantiomers self-assemble into an enantiomorphous packing pattern, which belongs to the chiral plane group *p*6 (Figure 2), which is one out of a total of five chiral plane groups.[24,59]

The transfer of molecular chirality into monolayer chirality is also expressed by the nonrandom orientation of the adlayer domains with respect to the graphite substrate underneath, where symmetry axes of domains of *R*-OPV3T and *S*-OPV3T are rotated over the same absolute angle, but with opposite sign (see Figure 2 and Supporting Information S2). Monolayers composed of solely thymidine molecules at the 1-octanol/HOPG interface were never observed.

**Self-Assembly of a Mixture of OPV3T and Thymidine: STM and Modeling.** In the second phase of the study, we investigated the effect of thymidine on the self-assembly of chiral OPV3T at the liquid/solid interface. In practice, we have dropcast premixed solutions of the OPV3T enantiomers and the thymidine enantiomers to minimize kinetic effects. Upon dropcasting, patterns arise that differ from those formed by pure OPV enantiomers. At this stage, we just introduce these new patterns and comment on some structural aspects, while in the next sections the importance and effect of solution composition (concentration, ratio) on the outcome of the self-assembly process will be discussed.

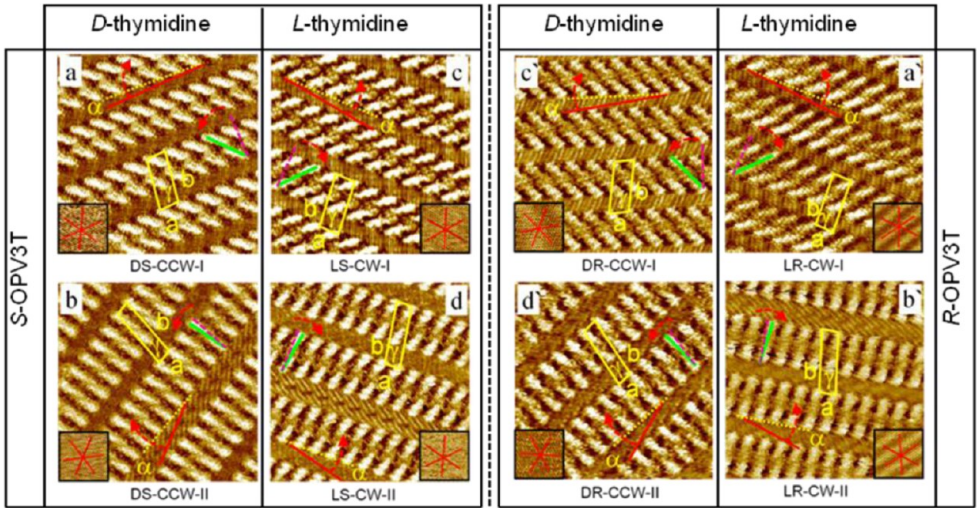


**Figure 3.** STM-images of monolayers formed from a solution of *S*-OPV3T or *R*-OPV3T with D- or L-thymidine at the 1-octanol/graphite interface. The labels underneath the STM images refer to the solution composition (e.g., "DS" refers to D-thymidine and *S*-OPV3T) and type of arrangement on the surface; "CCW" (counter clockwise) and "CW" (clockwise) refer to the orientation of the dimers with respect to the short axis of the molecular rows. "I" indicates that the dimers are rotated over a large angle with respect to the short lamella axis, while "II" refers to dimers that are nearly parallel to the short lamella axis. [OPV] = 1 mM in all cases. [Thymidine] = 1 mM for a, c, a′, and c′. [Thymidine] = 10 mM for b, d, b′, and d′. Insets are STM images of graphite underneath the respective monolayer. The red solid lines reflect main symmetry axes of graphite, and the yellow dotted lines run parallel to the unit cell vector *a*. The size of all images is 18 × 18 $nm^2$. Green solid lines cover a dimer. Purple dotted lines show the short lamella axis.

Typically, rows or lamellae of dimer-like bright rods appear. The dimensions of a single bright rod correspond to the oligo-(*p*-phenylenevinylene) unit of OPV3T. There are no features in the images that can be assigned unequivocally to the thymidine units, similar to our previous study of the self-assembly of achiral OPV3T with thymidine.[55] All possible combinations of OPV3T enantiomers and thymidine enantiomers were investigated (Figure 3). The unit cell parameters (*a*, *b*, and $\gamma$) and the angle $\alpha$ between the short lamella axis and the main symmetry directions (i.e., the $\langle 11\bar{2}0 \rangle$ directions) of HOPG are summarized in Table 1. The mixtures form several types of what we will call "dimer"-like patterns. In this Article, "dimer" only refers to the appearance of the OPV3T units. The dimers can be rotated clockwise (CW) or counterclockwise (CCW) with respect to the short lamella axis. The combinations containing D-thymidine produce CCW dimers and those containing L-thymidine give rise to CW dimers, independent of the chirality of the OPV3T enantiomer. Furthermore, any combination including OPV3T and thymidine can lead to two different types of dimers, identified as type "I" or type "II". "I" indicates that the dimers are rotated over a large angle with respect to the short lamella axis, while "II" refers to dimers that are nearly parallel to the short lamella axis. On the basis of this information, we labeled the dimers of all combinations of chiral OPV3T and thymidine as shown in Figure 3. High-resolution STM images, taking molecular structures and unit cell parameters into account, show the formation of diastereomeric as well as enantiomorphous patterns. The latter mirror-image patterns also have opposite orientations with respect to the main symmetry axis of the substrate (Table 1). There are four enantiomorphous pairs: DS-CCW-I and LR-CW-I; DS-CCW-II and LR-CW-II; DR-CCW-I and LS-CW-I; and DR-CCW-II and LS-CW-II. As discussed above, the pattern and domain chirality are dominated by the chirality of thymidine instead of the chirality of OPV3T.

**Table 1. Orientation Angle of the Short Lamella Axis with Respect to HOPG Main Symmetry Directions ($\alpha$) and Unit Cell Parameters (*a*, *b*, and $\gamma$) of CCW and CW Dimers**

| | $\alpha$ (deg) | *a* (nm) | *b* (nm) | $\gamma$ (deg) |
|---|---|---|---|---|
| DS-CCW-I | +7 ± 2 | 1.9 ± 0.1 | 4.5 ± 0.1 | 93 ± 2 |
| LS-CW-I | −8 ± 2 | 1.8 ± 0.1 | 4.7 ± 0.2 | 92 ± 5 |
| DS-CCW-II | +15 ± 3 | 1.5 ± 0.1 | 5.5 ± 0.3 | 97 ± 4 |
| LS-CW-II | −15 ± 2 | 1.5 ± 0.1 | 5.5 ± 0.2 | 97 ± 2 |
| DR-CCW-I | +9 ± 2 | 1.9 ± 0.1 | 4.8 ± 0.2 | 91 ± 4 |
| LR-CCW-I | −7 ± 4 | 1.9 ± 0.1 | 4.8 ± 0.1 | 93 ± 3 |
| DR-CCW-II | +16 ± 2 | 1.6 ± 0.1 | 5.6 ± 0.2 | 98 ± 2 |
| LR-CW-II | −16 ± 1 | 1.6 ± 0.1 | 5.5 ± 0.2 | 96 ± 4 |

The appearance of the type I and type II dimers depends on the solution composition. Therefore, the transformation from rosettes to dimers upon addition of thymidine was investigated in detail by changing the solution ratio (*R*) of D-thymidine or L-thymidine versus *S*-OPV3T (*R* = [thymidine]:[*S*-OPV3T]), for a constant concentration of *S*-OPV3T. Besides the transformation from rosettes to dimers, a molar ratio-dependent pattern transformation from dimer I to dimer II was observed.

Figure 4a−c shows a set of representative STM images at different ratios *R* at a constant *S*-OPV3T concentration for the mixture of D-thymidine and *S*-OPV3T (abbreviated as DS mixture). Figure 4d shows the population of the different structures as a function of *R*. The steep drop in fraction of rosettes and the concomitant rise in the fraction of dimers at low *R* suggests a strong substrate-driven 1:1 complexation (see Figure 4d). The fraction of rosettes decreases with increasing *R*, and from *R* = 2 on, no rosettes can be observed. While a decrease of the population of rosettes goes hand in hand with an increase in fraction of dimer-like features, there is a clear different ratio dependence for DS-CCW-I as compared to DS-CCW-II dimers. Initially, DS-CCW-I dimers are formed almost exclusively, reaching a maximum at about *R* = 1. At higher ratios, the population of DS-CCW-II increases at the expense of

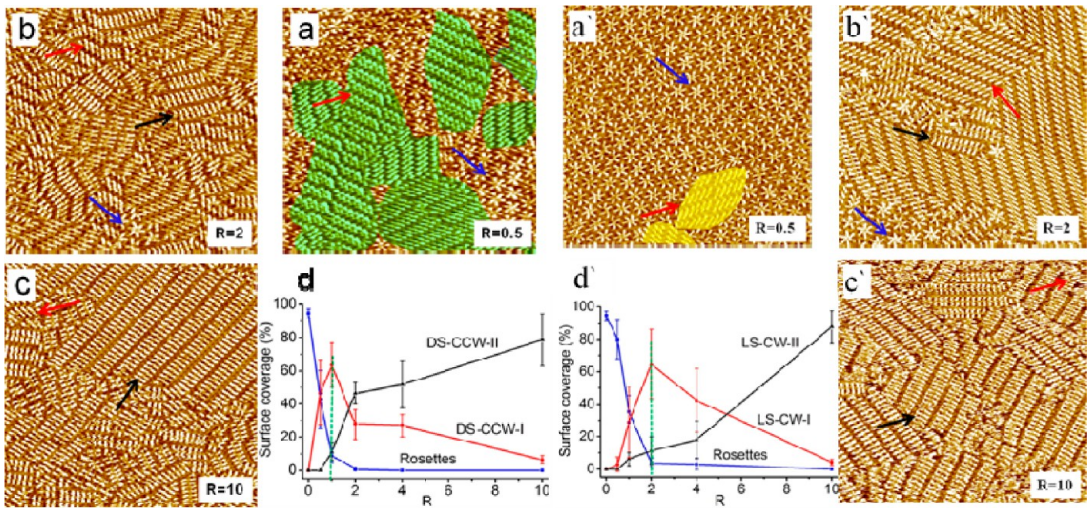


**Figure 4.** (a−c, a′−c′) STM-images of diastereomeric monolayers formed from solutions containing *S*-OPV3T and enantiopure thymidine at the 1-octanol/HOPG interface at different ratios (*R*) of thymidine versus *S*-OPV3T (*R* = [thymidine]:[*S*-OPV3T]) for a constant concentration of *S*-OPV3T (1.0 mM). (a−c) D-Thymidine and *S*-OPV3T: (a) *R* = 0.5, $I_{set}$ = 0.75 nA, $V_{set}$ = −0.32 V. (b) *R* = 2.0, $I_{set}$ = 0.728 nA, $V_{set}$ = −0.247 V. (c) *R* = 10, $I_{set}$ = 0.65 nA, $V_{set}$ = −0.25 V. (a′−c′) L-Thymidine and *S*-OPV3T: (a′) *R* = 0.5, $I_{set}$ = 0.397 nA, $V_{set}$ = −0.43 V. (b′) *R* = 2.0, $I_{set}$ = 0.20 nA, $V_{set}$ = −0.23 V. (c′) *R* = 10. $I_{set}$ = 0.75 nA, $V_{set}$ = −0.30 V. The blue arrows point to rosettes, the red arrows point to type I dimers, and the black arrows point to type II dimers. Size of all STM images is 65 × 65 $nm^2$. (d,d′) Surface coverage (%) of rosettes and the dimers as a function of *R* for (d) D-thymidine and (d′) L-thymidine. The sum of the surface coverage does not always reach 100%, because defects are not included.

DS-CCW-I. The monolayers are composed almost exclusively of DS-CCW-II dimers at very high R (Supporting Information S3).

As compared to the previous results, the diastereomeric monolayer mixtures of L-thymidine and *S*-OPV3T (abbreviated as LS mixture) seem to be very similar at first sight (Figure 4a′−d′). At very low *R*, rosettes are exclusively observed, while at higher ratios, LS-CW-I dimers are formed peaking at *R* ≈ 2, and being replaced by LS-CW-II dimers at even higher ratios (Supporting Information S3). However, there is a big difference at low *R* when comparing the surface coverage of rosettes and dimers formed by *S*-OPV3T with L- or D-thymidine. This difference is reflected in Figure 4a and a′, where the surface coverage of dimers is marked in green and yellow, respectively. Furthermore, Figure 5 compares the rosette surface coverage

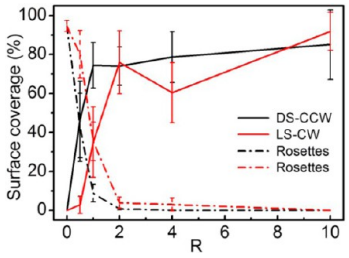


**Figure 5.** Surface coverage (%) of rosettes and dimers formed from a DS mixture (black) and dimers formed from a LS mixture (red) as a function of *R*. *R* = [thymidine]:[*S*-OPV3T]. [*S*-OPV3T] = 1.0 mM.

with the total dimer surface coverage (i.e., dimer I and dimer II) of DS mixtures, and its diastereomeric LS mixtures as a function of *R*. In case of DS mixtures, dimers are formed (and rosettes disappear) at lower *R* values as compared to LS mixtures. For example, at *R* = 0.5, there was already about 50% of the surface covered by dimers from the DS mixture, but only very few LS-dimers were found on the surface. Assuming that the self-assembly process occurs under equilibrium conditions, and that the "invisible" thymidine enantiomers are part of the monolayer, these results suggest that the interaction in DS assemblies might be stronger than that in LS assemblies or that DS assemblies are preferentially adsorbed.

One should note that the surface coverage of rosettes and dimers does not only depend on the ratio between thymidine and OPV3T in solution, but also on their concentration. Figure 6 shows the evolution of the number of dimers as a function of

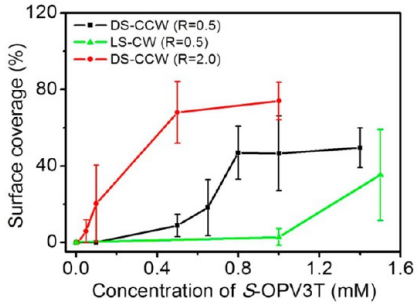


**Figure 6.** Surface coverage evolution of the total dimer species adsorbed from DS mixtures with *R* = 0.5 (black) and *R* = 2.0 (red) and the total dimers adsorbed from LS mixtures with *R* = 0.5 (green) as a function of the concentration of *S*-OPV3T.

the *S*-OPV3T concentration for DS (*R* = 0.5; *R* = 2) and LS (*R* = 0.5) mixtures. These experiments reveal three trends: (1) the dimer complex formation is favored for larger values of *R*, in agreement with the data in Figure 5; (2) at low solution concentrations, hardly any dimer complex is formed; and (3) the fraction of LS-dimers increases much slower than the fraction of the diastereomeric DS-dimers upon increasing the solution concentration, which is in line with the anticipated higher stability of the DS-dimers.

The trends observed in Figure 6 can be related to the existence of a number of solution and surface equilibrium processes. The question rises if the diastereomeric complex is

formed in solution or on the surface. In other words, does the presence of the achiral surface facilitate the formation and adsorption of one particular diastereomer, or is the preferred diastereomeric complex preformed in solution prior to self-assembling on the HOPG surface? Complex formation in solution was evaluated under the same conditions (solvent, concentration) as for the STM experiments by using NMR (Supporting Information S5). These experiments showed no indication for hydrogen-bonded thymidine/OPV3T complexes in solution, which means that the substrate plays a key role in this process. This is in line with the ability of the solvent (1-octanol) to compete with the solute for hydrogen bonding.[47]

**Molecular Modeling.** The pattern transformation from rosettes to dimers indicates that thymidine interacts with OPV on the surface.[55] STM images were analyzed in detail, and the unit cell parameters were used as input for molecular modeling studies.

The approach used for modeling the mechanistic aspects of chiral recognition and dimer formation involves a combination of molecular mechanics (MM) and molecular dynamics (MD) simulations. It was applied only to diastereomeric combinations of *S*-OPV3T and L- (or D-) thymidine molecules in a 2:1 ratio, but we expect the corresponding *R*-OPV3T-based monolayers to show a mirror imaged behavior. We have previously argued that the formation of a dense OPV3T adlayer on graphite is incompatible with all of the dodecyloxy side chains lying flat on the surface.[55] The STM measurements indeed indicate that one out of the three side chains of the OPV core is completely desorbed and solvated by the supernatant solution. As solvent molecules are not explicitly considered in the simulations, we removed one of the three side chains for the sake of simplicity. The other two chains partially adsorb on the graphite substrate, thereby contributing to the formation of the adlayer. Models for monolayers including 16 *S*-OPV3T and 8 L- (or D-) thymidine molecules were generated on top of a double layer of graphite, which was kept frozen (see the DS-CCW-I model in Figure 7). The calculations were carried out maintaining the lattice parameters to the STM-determined values for L(D)S-(C)CW-I and L(D)S-(C)CW-II.

The modeling studies indicate that the formation of coassemblies involving *S*-OPV3T and thymidine molecules on graphite proceeds similarly to what has been previously reported for the corresponding monolayers made of achiral OPV3T (A-OPV3T) in combination with thymidine.[55] In both cases, the codeposition of OPV3T and thymidine occurs in two possible ways, referred to as "linear inclusion" and "lateral inclusion" hereafter, and depicted schematically in Figure 8 in the case of the DS combination. In the linear inclusion scenario, two OPV3T molecules belonging to neighbor dimers align along their longitudinal axes and are separated by two hydrogen-bonded thymidine molecules lying in the interstitial space. Such a spatial arrangement of the molecules yields a relatively large (as compared to the lateral inclusion model) value for the short axis lattice parameter, which allows for partial interdigitation of the long terminal alkyl chains. In the lateral inclusion case, thymidine molecules intercalate within the OPV3T rows, resulting in alternated OPV3T-thymidine sequences. This supramolecular organization favors interactions between hydrogen-bonding sites and promotes short lateral contacts. As a result, the unit cell is characterized by a small length along the short axis, while the long axis elongates to reduce the repulsion between the alkyl chains.

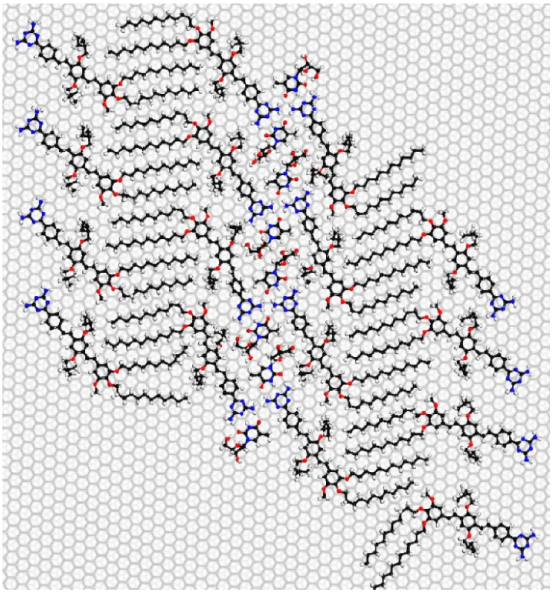

**Figure 7.** Molecular model for the self-assembled monolayer of D-thymidine/*S*-OPV3T on graphite (model DS-CCW-I, see text).

We next turn to the energetic aspects of the assemblies, with a 2-fold objective. On one hand, we assess the resolving capability of a thymidine enantiomer with respect to OPV3T; on the other hand, we compare the relative stabilities of the two models proposed above as a function of the molecular ratio between thymidine and OPV3T molecules. We demonstrated earlier that A-OPV3T and thymidine coadsorb on graphite into monolayers featuring dense molecular packing but with disordered, partially desorbed alkyl chains.[55] That organization turns out to be more stable than an ordered monolayer structure where the alkyl chains would lie completely flat on the surface as this would yield a less dense layer. Both types of dimers are stable entities under the experimental conditions; that is, for a certain concentration/ratio range, no conversion of one type of dimer into the other one is observed as a function of time. Type I dimers are also not kinetically trapped species, as adding extra thymidine to the supernatant solution leads to an overall increase of type II dimers (Supporting Information S4). We speculate that under such conditions, the type II dimers are further stabilized by additional interactions with thymidine molecules, alhough not in the plane of the monolayer. An alternative explanation is that type I dimers are initially better stabilized in a "sea" of rosettes, although there is no experimental proof for this. The total interaction energies per surface area are summarized in Table 2.

Importantly, the modeling studies prove that the coassemblies composed of *S*-OPV3T and D-thymidine are more stable (larger absolute values for the total interaction energies, Table 2) than the diastereomeric coassemblies formed with L-thymidine counterparts. The calculations suggest that the difference in stability is related to the conformation of the thymidine molecule on the surface. In the DS assembly, both the thymidine−OPV3T intermolecular interactions and the thymidine−graphite interactions are optimal: the thymine units adsorb almost perfectly flat-on the substrate, which maximizes the CH−$\pi$ and $\pi$−$\pi$ interactions. In contrast, in the LS assembly, the most stable thymidine−OPV3T arrangement implies that the thymidine molecule is distorted with respect to adsorption on graphite; in particular the thymine unit is tilted

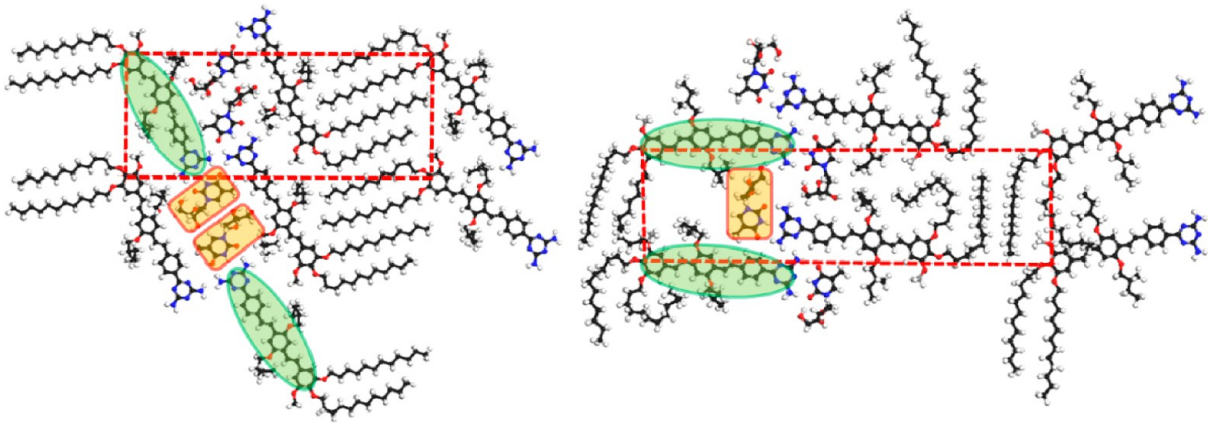

**Figure 8.** Unit cells (red dashed lines) and representation of linear inclusion for model DS-CCW-I (left) or lateral inclusion for model DS-CCW-II (right) assemblies.

**Table 2. Total Interaction Energies Averaged over the MD Simulations for the Different Assemblies Investigated**

| model | totel interaction energy (kJ mol$^{-1}$ nm$^{-2}$) | standard deviation (kJ mol$^{-1}$ nm$^{-2}$) |
|---|---|---|
| DS-CCW-I | −987.0 | 12.7 |
| DS-CCW-II | −1036.4 | 13.7 |
| DL-CW-I | −920.9 | 12.3 |
| DL-CW-II | −955.6 | 13.7 |

with respect to the graphite plane, which decreases the interaction energy with the substrate. This difference in the adsorption geometry of the two thymidine enantiomers is illustrated in Figure S7. In other words, the D-thymidine molecules can simultaneously interact favorably with the *S*-OPV3T molecules (via H-bonds) and the substrate, whereas the L-thymidine molecules "must make a choice": optimal H-bonding with *S*-OPV3T implies tilted adsorption on the substrate. The L-thymidine molecule can adsorb in the most favorable way only if it is associated with the *R*-OPV3T species. These results thus support the view that an OPV3T enantiomer can act as resolving agent for the separation of the thymidine enantiomers, which we explore experimentally in the next step.

**Resolving Thymidine Enantiomers by Using a Chiral OPV3T.** The preferred association of thymidine with a specific OPV3T enantiomer provides the opportunity to explore the preferential adsorption of one of the thymidine enantiomers from a racemate of thymidines. Because the domain chirality upon coadsorption of OPV3T and thymidine is ruled by the absolute configuration of thymidine, STM can be used directly to evaluate enantioselective adsorption of thymidine enantiomers at the liquid/solid interface (Figure 9).

We first evaluated a solution composed of a thymidine racemate (*rac*-thymidine) with [*S*-OPV3T] = 1 mM and [D-thymidine]:[L-thymidine]:[*S*-OPV3T] = 1:1:2. A typical image of the adlayer adsorbed from this three-component mixture is shown in Figure 10a. The domains with CCW dimers resulting from coadsorption with D-thymidine are highlighted in green, while the domains with CW dimers resulting from coadsorption with L-thymidine are indicated in yellow. The remaining surface is covered with rosettes and disordered structures. It is clear that for a mixture of *S*-OPV3T and both thymidine enantiomers, the surface is covered with CCW as well as CW diastereomeric dimers. Because of the higher coverage of CCW dimers (∼37%) as compared to CW dimers (∼2%), one can conclude that DS dimers preferentially form on the surface. For a solution of *rac*-thymidine with *R*-OPV3T ([D-thymidine]:[L-thymidine]:[*R*-OPV3T] = 1:1:2, [*R*-OPV3T] = 1 mM), a clear preference for CW domains is found (Figure 10b). The surface is covered with ∼42% of CW dimers and only ∼5% of the diastereomeric CCW dimers, confirming that LR dimers are preferentially adsorbed over DR dimers in the latter case.

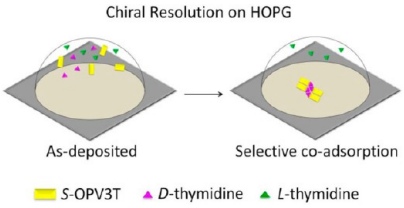


**Figure 9.** The mechanism of enantioselective adsorption of thymidine on HOPG by using *S*-OPV3T enantiomer as a resolving agent.

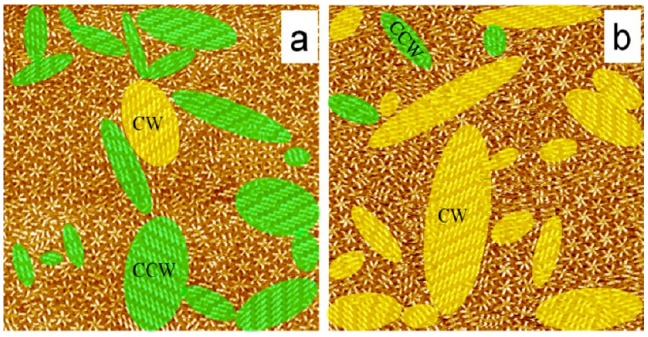


**Figure 10.** STM-images at the 1-octanol/HOPG interface of (a) *S*-OPV3T with thymidine racemate, and [*rac*-thymidine]:[*S*-OPV3T] = 1. $I_{set}$ = 0.65 nA, $V_{set}$ = −0.30 V. (b) *R*-OPV3T with thymidine racemate, and [*rac*-thymidine]:[*R*-OPV3T] = 1. $I_{set}$ = 0.60 nA, $V_{set}$ = −0.30 V. [OPV3T] = 1 mM. Size of all STM images is 80 × 80 nm$^2$.

So, the chiral OPV3T molecules can conceptually be used as resolving agent and partly resolve thymidine enantiomers at the 1-octanol/HOPG interface. Because there is no preorganization and complex formation in solution under the experimental conditions, the diastereomeric complex formation must occur on the surface. In other words, chiral resolution is mediated by the presence of the achiral surface, facilitating the formation of

hydrogen-bonded thymidine/*S*-OPV3T complexes and adsorption of one particular diastereomer.

In the next phase, different molar ratios with a constant *S*-OPV3T concentration were explored to optimize the resolving conditions (Supporting Information S6). For several mixtures of *S*-OPV3T with the thymidine racemate, the amount of diastereomeric DS- and LS-dimers was calculated for different solution ratios between *rac*-thymidine and *S*-OPV3T (Figure 11a). The resulting curves for DS-complexes and LS-complexes

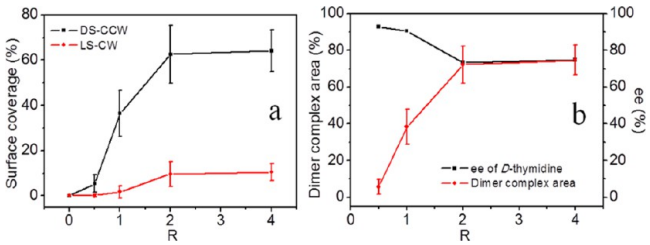


**Figure 11.** Detailed analysis of solution mixtures of *rac*-thymidine and *S*-OPV3T. (a) Surface coverage (%) of diastereomeric DS and LS dimer complex as a function of the molar ratio *R*. (b) Surface ee (%) of D-thymidine and dimer complex area (%) as a function of molar ratio. *R* = [*rac*-thymidine]:[*S*-OPV3T]. [*S*-OPV3T] = 1 mM.

adsorbed from *rac*-thymidine mixed with *S*-OPV3T show the same tendency as compared to mixtures of D-thymidine and *S*-OPV3T or L-thymidine and *S*-OPV3T. The surface coverage of both dimer complexes increases upon increasing *R* (*R* = [*rac*-thymidine]:[S-OPV3T] and [S-OPV3T] = 1.0 mM), and both curves reach a plateau after approximately *R* = 2 (Figure 11a). The surface covered by DS- and LS-complexes, next to the coexistence of rosettes or disordered phases, was determined to evaluate the fraction of the surface area (A) active in chiral resolution (the resolving surface area). The resolving surface area percentage can be defined by the area occupied by DS-dimers ($A_{DS}$) divided by the total surface area of the HOPG substrate ($A_{total}$). To assess the efficiency of the resolving surface, two contributions have to be taken into account. First, the enantiomeric excess (ee) of D-thymidine on the surface was calculated ($(A_{DS} - A_{LS})/(A_{DS} + A_{LS})$), assuming formation of a 1:1 complex. Second, the percentage (%) of the dimer complex area was defined as ($(A_{DS} + A_{LS})/A_{total}$), as a function of *R* as well (Figure 11b). The occupied surface area by thymidine/*S*-OPV3T complexes increases with increasing *R* and reaches a plateau at *R* = 2. The ee of D-thymidine decreases with increasing *R* and levels off at *R* = 2. The maximum ee is about 93%, and the minimum is about 74%. From the experimental data, we can conclude that for higher *R* more dimer complexes will form on the surface but at the expense of the efficiency of the resolving surface area, as seen from a decreasing ee.

We also investigated the concentration effect on the resolving process. At *R* = 0.5, increasing the concentration of *S*-OPV3T from 1.0 to 1.6 mM resulted in a large increase in the occupied surface by dimers (from 6% to 61%) and a relative small decrease in the ee of D-thymidine (from 93% to 78%) (Supporting Information S7). From the molar ratio and concentration dependency, one concludes that a relatively low molar ratio (*R*) and high overall concentration leads to a good compromise between yield and ee for resolving thymidine enantiomers via chiral OPV3T at the 1-octanol/HOPG interface. Note that "yield" refers to the fraction of the graphite substrate covered by thymidine/OPV3T dimer complexes. It does not refer to the solution composition. Under the experimental conditions, only a small fraction of thymidine molecules are coadsorbed on the surface (less than 0.001%).[60]

## ■ CONCLUSIONS

We have explored the self-assembly of mixtures of an enantiopure oligo-(*p*-phenylenevinylene) derivative (OPV3T) and enantiopure thymidine or its racemate at the liquid/solid interface. STM was used to visualize the molecular nanopatterns at the interface between the substrate, that is, graphite, and the solvent, that is, 1-octanol. Molecular mechanics and dynamics simulations provided insight into the structural aspects of the nanopatterns. Addition of thymidine drastically changes the supramolecular motifs of the chiral OPV3T derivatives. Rosettes are converted into dimers, which was attributed to the coadsorption of thymidine, leading to the formation of diastereomeric complexes. Investigation of all possible combinations of OPV3T and thymidine enantiomers revealed surface-mediated preferential diastereomeric complex formation and adsorption. This was applied to bias the adsorption of thymidine enantiomers from the solution racemate by using a chiral OPV3T enantiomer as resolving agent. Molar ratio and concentration of the components play a key role in the surface-mediated resolution process.

These studies shine light on the complexity of adsorption processes at the liquid/solid interface for multicomponent mixtures, and highlight the role of achiral atomically flat surfaces as potential supports for enantioselective adsorption processes, potentially leading to the separation of enantiomers. In particular, in solution the intermolecular recognition is less specific due to many possible conformations, while it is more specific due to lower dimensionality at a surface.

## ■ EXPERIMENTAL SECTION

**Synthesis.** The synthesis of *S*-OPV3T has been reported previously[61] while the synthesis of *R*-OPV3T is analogous to *S*-OPV3T and will be reported elsewhere.

**Scanning Tunneling Microscopy.** All STM experiments were carried out at 20−25 °C. Experiments were performed using a PicoSPM microscope (Agilent). Tips were mechanically cut from Pt−Ir wire (80:20 alloy, diameter 0.25 mm). Prior to imaging, the OPV3T and/or the thymidines were dissolved in 1-octanol (anhydrous, 99+%, Sigma-Aldrich), and a drop of the solution was applied onto a freshly cleaved surface of graphite (HOPG, grade ZYB, Advanced Ceramics Inc., Cleveland, OH). The STM investigations were then performed at the liquid/solid interface at least 90 min after drop casting. Images are recorded in the constant current mode. $V_{set}$ refers to the sample bias. The graphite lattice was recorded by lowering the sample bias immediately after obtaining images of the monolayer. Drift effects were corrected via scanning probe image processor (SPIP) software (Image Metrology ApS). To ensure a statistical relevant approach when analyzing the ratio between rosette and dimer domains, for each "*R*", different samples were prepared and at least 15 large-scale images (80 × 80 nm$^2$) were selected randomly for statistical analysis. The surface coverage is calculated by counting the number of OPV units.

**Molecular Modeling.** The physisorption of the adlayers on graphite was modeled by means of a molecular mechanics/molecular dynamics (MM/MD) approach. The DREIDING[62] force field, as implemented in the FORCITE tool pack of Materials Studio, was used, because it is particularly adapted to account for the hydrogen bonds that promote the self-assembly of the molecules under investigation. The validity of the force field for studying H-bonded supramolecular systems has been proven previously for a similar system.[55] The force field calculations were performed on model systems including *S*-OPV3T and D/L-thymidine molecules in a 2:1 ratio deposited on graphite. The initial geometric configurations were

inspired from assembly models based on the STM measurements. These were then subjected to energy minimization at 0 K, releasing step by step all constraints imposed by the construction of the assemblies, followed by MD simulations in the NVT ensemble at 298 K for 1 ns. The long-range nonbonded interactions were turned off with a cubic spline cutoff set at 18 Å.

## ■ ASSOCIATED CONTENT

### Supporting Information

STM images, NMR spectra, and molecular modeling. This material is available free of charge via the Internet at http://pubs.acs.org.

## ■ AUTHOR INFORMATION


### Corresponding Author

roberto.lazzaroni@umons.ac.be; a.p.h.j.schenning@tue.nl; steven.defeyter@chem.kuleuven.be

### Present Addresses

[⊥]Laboratory of Functional Organic Materials, Eindhoven University of Technology, P.O. Box 513, 5600 MB Eindhoven, The Netherlands.

[#]School of Materials Science and Engineering, University of Science and Technology Beijing, No. 30 Xueyuan Road, Beijing 100083, China.


### Notes

The authors declare no competing financial interest.

## ■ ACKNOWLEDGMENTS

The research leading to these results has received funding from the European Community's Seventh Framework Programme under grant agreement no. NMP4-SL-2008-214340, project RESOLVE, the Interuniversity Attraction Pole program of the Belgian Federal Science Policy Office (IAP P7/05), the Fund of Scientific Research-Flanders (FWO), and the agency for the Promotion of Innovation by Science and Technology in Flanders (IWT). Research in Leuven is furthermore supported by GOA. Research in Mons is also supported by Région Wallonne (OPTI2MAT excellence program) and FNRS-FRFC. D.B. is an FNRS research director. We also thank Maarten Pouderoijen and Dr. Peter Korevaar for discussions.

## ■ REFERENCES


(1) Noorduin, W. L.; Izumi, T.; Millemaggi, A.; Leeman, M.; Meekes, H.; Van Enckevort, W. J. P.; Kellogg, R. M.; Kaptein, B.; Vlieg, E.; Blackmond, D. G. *J. Am. Chem. Soc.* **2008**, *130*, 1158−1159.

(2) Noorduin, W. L.; van der Asdonk, P.; Meekes, H.; van Enckevort, W. J. P.; Kaptein, B.; Leeman, M.; Kellogg, R. M.; Vlieg, E. *Angew. Chem., Int. Ed.* **2009**, *48*, 3278−3280.

(3) Ward, T. J.; Ward, K. D. *Anal. Chem.* **2012**, *84*, 626−635.

(4) Collins, A. N.; Sheldrake, G. N.; Crosby, J. *Chirality in Industry: The Commercial Manufacture and Applications of Optically Active Compunds*; John Wiley and Sons: Chichester, 1992.

(5) Gübitz, G., Schmid, M. G., Eds. *Biopharm. Drug Dispos.* **2001**, 291−336.

(6) Lorenzo, M. O.; Baddeley, C. J.; Muryn, C.; Raval, R. *Nature* **2000**, *404*, 376−379.

(7) Kesanli, B.; Lin, W. B. *Coord. Chem. Rev.* **2003**, *246*, 305−326.

(8) Dressler, D. H.; Mastai, Y. *Chirality* **2007**, *19*, 358−365.

(9) Paik, P.; Gedanken, A.; Mastai, Y. *J. Mater. Chem.* **2010**, *20*, 4085−4093.

(10) van Erp, T. S.; Caremans, T. P.; Dubbeldam, D.; Martin-Calvo, A.; Calero, S.; Martens, J. A. *Angew. Chem., Int. Ed.* **2010**, *49*, 3010−3013.

(11) Gellman, A. J.; Horvath, J. D.; Buelow, M. T. *J. Mol. Catal. A: Chem.* **2001**, *167*, 3−11.

(12) Paci, I.; Szleifer, I.; Ratner, M. A. *J. Am. Chem. Soc.* **2007**, *129*, 3545−3555.

(13) Sancho, R.; Minguillon, C. *Chem. Soc. Rev.* **2009**, *38*, 797−805.

(14) Gübitz, G.; Schmid, M. G. *Biopharm. Drug Dispos.* **2001**, *22*, 291−336.

(15) Yamamoto, C.; Okamoto, Y. Practical resolution of enantiomers by high-performance liquid chromatography. In *Enantiomer Separation*; Toda, F., Ed.; Springer: Netherlands, 2004; pp 301−322.

(16) Xu, H.; Saletra, W. J.; Iavicoli, P.; Van Averbeke, B.; Ghijsens, E.; Mali, K. S.; Schenning, A. P. H. J.; Beljonne, D.; Lazzaroni, R.; Amabilino, D. B.; De Feyter, S. *Angew. Chem., Int. Ed.* **2012**, *51*, 11981−11985.

(17) Weissbuch, I.; Berfeld, M.; Bouwman, W.; Kjaer, K.; AlsNielsen, J.; Lahav, M.; Leiserowitz, L. *J. Am. Chem. Soc.* **1997**, *119*, 933−942.

(18) Ahmadi, A.; Attard, G.; Feliu, J.; Rodes, A. *Langmuir* **1999**, *15*, 2420−2424.

(19) Jacques, J.; Collet, A.; Wilen, S. H. *Enantiomers, Racemates, and Resolutions*; Krieger: FL, 1981.

(20) Schonherr, H.; Crego-Calama, M.; Vancso, G. J.; Reinhoudt, D. N. *Adv. Mater.* **2004**, *16*, 1416−1420.

(21) Yuan, Q. H.; Yan, C. J.; Yan, H. J.; Wan, L. J.; Northrop, B. H.; Jude, H.; Stang, P. J. *J. Am. Chem. Soc.* **2008**, *130*, 8878−8879.

(22) Stohr, M.; Boz, S.; Schar, M.; Nguyen, M. T.; Pignedoli, C. A.; Passerone, D.; Schweizer, W. B.; Thilgen, C.; Jung, T. A.; Diederich, F. *Angew. Chem., Int. Ed.* **2011**, *50*, 9982−9986.

(23) Eckhardt, C. J.; Peachey, N. M.; Swanson, D. R.; Takacs, J. M.; Khan, M. A.; Gong, X.; Kim, J. H.; Wang, J.; Uphaus, R. A. *Nature* **1993**, *362*, 614−616.

(24) Plass, K. E.; Grzesiak, A. L.; Matzger, A. J. *Acc. Chem. Res.* **2007**, *40*, 287−293.

(25) Kuzmenko, I.; Weissbuch, I.; Gurovich, E.; Leiserowitz, L.; Lahav, M. *Chirality* **1998**, *10*, 415−424.

(26) Perez-Garcia, L.; Amabilino, D. B. *Chem. Soc. Rev.* **2007**, *36*, 941−967.

(27) Perez-Garcia, L.; Amabilino, D. B. *Chem. Soc. Rev.* **2002**, *31*, 342−356.

(28) Bohringer, M.; Morgenstern, K.; Schneider, W. D.; Berndt, R. *Angew. Chem., Int. Ed.* **1999**, *38*, 821−823.

(29) Mastai, Y. *Chem. Soc. Rev.* **2009**, *38*, 772−780.

(30) Horvath, J. D.; Koritnik, A.; Kamakoti, P.; Sholl, D. S.; Gellman, A. J. *J. Am. Chem. Soc.* **2004**, *126*, 14988−14994.

(31) Nakanishi, T.; Banno, N.; Matsunaga, M.; Asahi, T.; Osaka, T. *Colloids Surf., A* **2006**, *284*, 270−275.

(32) Liu, N.; Haq, S.; Darling, G. R.; Raval, R. *Angew. Chem., Int. Ed.* **2007**, *46*, 7613−7616.

(33) Elemans, J.; De Cat, I.; Xu, H.; De Feyter, S. *Chem. Soc. Rev.* **2009**, *38*, 722−736.

(34) Weckesser, J.; de Vita, A.; Barth, J. V.; Cai, C.; Kern, K. *Phys. Rev. Lett.* **2001**, *87*, 096101−096104.

(35) Fang, H. B.; Giancarlo, L. C.; Flynn, G. W. *J. Phys. Chem. B* **1998**, *102*, 7311−7315.

(36) Yoon, J. K.; Son, W. J.; Kim, H.; Chung, K. H.; Han, S.; Kahng, S. J. *Nanotechnology* **2011**, *22*, 275705.

(37) Stepanow, S.; Lin, N.; Vidal, F.; Landa, A.; Ruben, M.; Barth, J. V.; Kern, K. *Nano Lett.* **2005**, *5*, 901−904.

(38) Huang, T.; Hu, Z. P.; Zhao, A. D.; Wang, H. Q.; Wang, B.; Yang, J. L.; Hou, J. G. *J. Am. Chem. Soc.* **2007**, *129*, 3857−3862.

(39) (a) Chen, Q.; Richardson, N. V. *Nat. Mater.* **2003**, *2*, 324−328. (b) Blankenburg, S.; Schmidt, W. G. *Phys. Rev. Lett.* **2007**, *99*, 196107. (c) Roth, C.; Passerone, D.; Ernst, K. H. *Chem. Commun.* **2010**, *46*, 8645−8647.

(40) Liu, J.; Chen, T.; Deng, X.; Wang, D.; Pei, J.; Wan, L. J. *J. Am. Chem. Soc.* **2011**, *133*, 21010−21015.

(41) Mark, A. G.; Forster, M.; Raval, R. *ChemPhysChem* **2011**, *12*, 1474−1480.

(42) Iavicoli, P.; Xu, H.; Feldborg, L. N.; Linares, M.; Paradinas, M.; Stafstrom, S.; Ocal, C.; Nieto-Ortega, B. L.; Casado, J.; Lopez Navarrete, J. T.; Lazzaroni, R.; De Feyter, S.; Amabilino, D. B. *J. Am. Chem. Soc.* **2010**, *132*, 9350−9362.

(43) Bombis, C.; Weigelt, S.; Knudsen, M. M.; Norgaard, M.; Busse, C.; Laegsgaard, E.; Besenbacher, F.; Gothelf, K. V.; Linderoth, T. R. *ACS Nano* **2010**, *4*, 297−311.
(44) Xu, H.; Wolffs, M.; Tomovic, Z.; Meijer, E. W.; Schenning, A. P. H. J.; De Feyter, S. *CrystEngComm* **2011**, *13*, 5584−5590.
(45) Kuhnle, A.; Linderoth, T. R.; Hammer, B.; Besenbacher, F. *Nature* **2002**, *415*, 891−893.
(46) Veling, N.; van Hameren, R.; van Buul, A. M.; Rowan, A. E.; Nolte, R. J. M.; Elemans, J. *Chem. Commun.* **2012**, *48*, 4371−4373.
(47) Katsonis, N.; Xu, H.; Haak, R. M.; Kudernac, T.; Tomovic, Z.; George, S.; Van der Auweraer, M.; Schenning, A.; Meijer, E. W.; Feringa, B. L.; De Feyter, S. *Angew. Chem., Int. Ed.* **2008**, *47*, 4997−5001.
(48) Parschau, M.; Kampen, T.; Ernst, K. H. *Chem. Phys. Lett.* **2005**, *407*, 433−437.
(49) Parschau, M.; Romer, S.; Ernst, K. H. *J. Am. Chem. Soc.* **2004**, *126*, 15398−15399.
(50) Masini, F.; Kalashnyk, N.; Knudsen, M. M.; Cramer, J. R.; Laegsgaard, E.; Besenbacher, F.; Gothelf, K. V.; Linderoth, T. R. *J. Am. Chem. Soc.* **2011**, *133*, 13910−13913.
(51) Fasel, R.; Parschau, M.; Ernst, K. H. *Nature* **2006**, *439*, 449−452.
(52) Haq, S.; Liu, N.; Humblot, V.; Jansen, A. P. J.; Raval, R. *Nat. Chem.* **2009**, *1*, 409−414.
(53) De Cat, I.; Guo, Z. X.; George, S. J.; Meijer, E. W.; Schenning, A. P. H. J.; De Feyter, S. *J. Am. Chem. Soc.* **2012**, *134*, 3171−3177.
(54) Ernst, K. H. *Origins Life Evol. Biospheres* **2010**, *40*, 41−50.
(55) Guo, Z. X.; De Cat, I.; Van Averbeke, B.; Lin, J. B.; Wang, G. J.; Xu, H.; Lazzaroni, R.; Beljonne, D.; Meijer, E. W.; Schenning, A. P. H. J.; De Feyter, S. *J. Am. Chem. Soc.* **2011**, *133*, 17764−17771.
(56) Miura, A.; Jonkheijm, P.; De Feyter, S.; Schenning, A. P. H. J.; Meijer, E. W.; De Schryver, F. C. *Small* **2005**, *1*, 131−137.
(57) Jonkheijm, P.; Miura, A.; Zdanowska, M.; Hoeben, F. J. M.; De Feyter, S.; Schenning, A.; De Schryver, F. C.; Meijer, E. W. *Angew. Chem., Int. Ed.* **2004**, *43*, 74−78.
(58) Minoia, A.; Guo, Z. X.; Xu, H.; George, S. J.; Schenning, A. P. H. J.; De Feyter, S.; Lazzaroni, R. *Chem. Commun.* **2011**, *47*, 10924−10926.
(59) Barlow, S. M.; Raval, R. *Surf. Sci. Rep.* **2003**, *50*, 201−341.
(60) We did not evaluate the power of thymidine to resolve OPV3T racemate. STM cannot be used to monitor the enantioselective adsorption of OPV3T enantiomers as the chiral expression of the thymidine/OPV3T complexes is dominated by the absolute configuration of thymidine.
(61) Jonkheijm, P.; Hoeben, F. J. M.; Kleppinger, R.; van Herrikhuyzen, J.; Schenning, A. P. H. J.; Meijer, E. W. *J. Am. Chem. Soc.* **2003**, *125*, 15941−15949.
(62) Mayo, S. L.; Olafson, B. D.; Goddard, W. A. *J. Phys. Chem.* **1990**, *94*, 8897−8909.